Available online at www.sciencedirect.com

SciVerse ScienceDirect

Procedia CIRP 8 (2013) 51 – 56

www.elsevier.com/locate/procedia

14th CIRP Conference on Modeling of Machining Operations (CIRP CMMO)

A Gear Cutting Predictive Model Using the Finite Element Method

W. Liu[a], D. Ren[a], S. Usui[a], J. Wadell[a], T. D. Marusich[a]*

[a]*Third Wave Systems, 6475 City West Parkway, Minneapolis MN 55344, USA*

* Corresponding author. Tel.: +1-952-832-5515; fax: +1-952-844-0202. *E-mail address*: sales@thirdwavesys.com.

Abstract

Current processes for producing transmission gears involve hobbing, milling or shaping of a forged stock to obtain the gear shape. Gears are typically formed by hobbing tools made from solid tooling material, such as tungsten carbide, and have dozens of teeth. The gear hobbing process entails several teeth in cut simultaneously. Generation of in-volute tooth profiles results in varying chip loads from pass to pass. In this paper, details are provided for a finite element-based model of gear hobbing and milling processes. The model explicitly meshes gear cutter geometries with dozens of teeth. These cutters are used to simulate the complicated kinematic motion between tool and workpiece. Thermo-mechanical coupled calculations within an explicit dynamic formulation are per-formed on the tool and workpiece during chip removal. The complex geometry of involute tooth profiles results in complicated contact scenarios on the evolving workpiece geometry during tooth profile generation. Tooth-workpiece-chip contact is enforced rigorously and is particularly complicated with the confined space of gear hobbing. Advanced adaptive meshing strategies are developed and employed to maintain the resolution of the tool-workpiece interaction while multiple teeth are in contact. Cutting forces, temperatures and stresses in the tool and workpiece are predicted for steel workpiece materials. Models are validated through a set of initially simplified experiments where incremental complexity is added, allowing for direct comparison between predicted and measured forces and chip shapes.

Selection and peer-review under responsibility of The International Scientific Committee of the "14th CIRP Conference on Modeling of Machining Operations" in the person of the Conference Chair Prof. Luca Settineri

Keywords: Modelling; Predictive; Hobbing

1. Introduction

Transmission gears can be produced by hobbing, milling, or shaping of a forged stock. The overall cycle times and component performance of a gear is dictated by many factors, including the amount of residual stresses, distortions, excess material generated during gear cutting, and following heat treatment processes. Due to the complex nature of the process and associated tooling, trial-and-error test methods for hob design are prohibitively expensive and time-consuming. It is desirable for tooling designers and manufacturing engineers to have a physics-based modeling tool for gear cutting.

The inherent complexity in gear cutting, such as sophisticated contact scenarios and nonlinear material behaviors under large plastic deformations and high strain rate, requires a substantial amount of research effort to understand the process. In this paper, a finite element-based model of gear hobbing and milling processes is developed. The model explicitly meshes gear cutter geometries and simulates the complicated kinematic motion between the tool and workpiece. Advanced adaptive meshing strategies are developed and employed to maintain the resolution of the tool-workpiece interaction while multiple teeth are in contact.

Cutting forces, temperatures in the tool and workpiece, and chip shapes are investigated for a steel workpiece material using the predictive model developed. A set of experiments were conducted for various cutting conditions, allowing for direct comparison between predicted and measured forces and chip shapes. Good correlations between the predictions and the experiments are observed.

Selection and peer-review under responsibility of The International Scientific Committee of the "14th CIRP Conference on Modeling of Machining Operations" in the person of the Conference Chair Prof. Luca Settineri

doi:10.1016/j.procir.2013.06.064

2. Theory

The finite element method has been widely used in engineering analyses. In this study, Third Wave AdvantEdge, a CAE software for simulating machining processes, is utilized. Dynamic equilibrium equations are solved by means of Lagrangian finite element formulations, and an explicit time integration algorithm is employed.

2.1. Finite Element Formulations

Considering the principle of virtual work, the weak form of the momentum equation by the Lagrangian description [1] is given as:

$$\begin{aligned}&\int_{B_0}\mathbf{P}_{n+1}:\nabla_0\boldsymbol{\eta}dV_0-\int_{B_0}\left(\mathbf{f}_{n+1}-\rho_0\mathbf{a}_{n+1}\right)\cdot\boldsymbol{\eta}dV_0,\\&-\int_{\partial B_{0\tau}}\bar{\mathbf{t}}_{n+1}\cdot\boldsymbol{\eta}dS_0=0\end{aligned}\qquad(1)$$

where P_{n+1} is the first Piola-Kirchhoff; the subscript n+1 refers to the time t_{n+1}; f_{n+1}, a_{n+1} and t_{n+1} are the body forces, accelerations and boundary tractions, respectively; ρ_0 is the mass density on the reference configuration B_0; η is an admissible virtual displacement field; and ∇_0 denotes the deformation gradient. After applying the spatial discretization, the finite element formulation in matrix form can be written as

$$\mathbf{M}\mathbf{a}_{n+1}+\mathbf{R}^{\mathrm{int}}_{n+1}=\mathbf{R}^{ext}_{n+1},\qquad(2)$$

where M is the mass matrix, a_{n+1} is the acceleration vector, and $\mathbf{R}^{ext}_{n+1}$ and $\mathbf{R}^{int}_{n+1}$ represent the external and internal force vectors, respectively. The central difference scheme is used for the time integration as

$$\begin{aligned}\mathbf{d}_{n+1}&=\mathbf{d}_n+\Delta t\mathbf{v}_n+\frac{1}{2}\Delta t^2\mathbf{a}_n\\\mathbf{a}_{n+1}&=\mathbf{M}^{-1}\left(\mathbf{R}^{ext}_{n+1}-\mathbf{R}^{\mathrm{int}}_{n+1}\right)\\\mathbf{v}_{n+1}&=\mathbf{v}_n+\frac{1}{2}\Delta t\left(\mathbf{a}_{n+1}+\mathbf{a}_n\right)\end{aligned},\qquad(3)$$

where d and v are the displacement and velocity vectors, respectively.

The plastic work in the workpice and the friction at the tool-chip interface can generate a large amount of heat in the machining process. Consequently, the temperature of the system might increase significantly. For the finite element solution of the heat transfer problem, the weak form in the current configuration B_t is considered,

$$\begin{aligned}&\int_{B_t}\rho c\dot{T}\eta dV+\int_{\partial B_{hq}}h\eta dS=\int_{B_t}\mathbf{q}\cdot\nabla\eta dV,\\&+\int_{B_t}s\eta dV\end{aligned}\qquad(4)$$

where ρ is the current mass density, c is the heat capacity, T is the temperature field, and $\mathbf{q}=-\mathbf{D}\cdot\nabla T$ is the heat flux in which D is the conductivity tensor. The frictional heat h is modeled as the boundary flux through the tool-chip interface. The heat generated by plastic work is considered as a heat source in the solid by assuming a fraction of the plastic work, given as $s=\beta W^P$, where β denotes the Taylor-Quinney coefficient. The explicit time integration is employed for the thermal problem as

$$\mathbf{T}_{n+1}=\mathbf{T}_n+\Delta t\mathbf{C}^{-1}\left(\mathbf{Q}_n-\mathbf{K}_n\mathbf{T}_n\right),\qquad(5)$$

where T is the temperature vector, and K and C are the conductivity and heat capacity matrix, respectively. Q is the heat source vector contributed from the friction and plastic work. The coupled thermo-mechanical equations are solved by a staggered procedure [2].

The stress update method developed by Cuitiño and Ortiz [3] is utilized for the constitutive model. To capture material behavior of metals under high speed machining, the flow stress is determined by

$$\sigma\left(\alpha,\dot{\alpha},T\right)=g\left(\alpha\right)\Theta\left(T\right)\Gamma\left(\dot{\alpha}\right)\qquad(6)$$

where $g(\alpha)$ is the isotropic strain hardening function, $\Theta(T)$ the thermal softening, and $\Gamma(\dot{\alpha})$ the rate sensitivity. α, $\dot{\alpha}$ and T denote the equivalent plastic strain, plastic strain rate and temperature, respectively. More details of the constitutive model in AdvantEdge are described by Man et al. [4].

To capture fine-scale features developed at the tool-chip interface such as shear localization bands and the secondary shear zone, adaptive remeshing strategies [2] are adopted. Meanwhile, deformation-induced element distortion in Lagrangian models is alleviated significantly. The adaptive remeshing is triggered once the element distortion reaches a critical value. Mesh refinement, improvement, and coarsening are automatically applied. In regions where materials experience plastic deformation, workpiece mesh is refined. On the other hand, the mesh coarsening procedure is applied in regions where plastic deformation is inactive in order to reduce the computation cost. The contact algorithm developed by Taylor and Flanagan [5] is employed in the FEA code to model the interaction between the tool and workpiece. Two surfaces that come into contact are treated as master and slave, the impenetrability is achieved by a predictor-corrector scheme.

2.2. Gear Hobbing Kinematics

Hobbing is generally considered as an accurate method of gear production [6]. Different from conventional milling, the kinematics of gear hobbing is governed by the rolling principle between the work gear and the hob [7]. Three-dimensional kinematics of gear hobbing is implemented in AdvantEdge for the predictive model. The code supports tool geometry import for various CAD formats such as STEP and VRML. Tool mesh is then generated for finite element analyses.

The final geometry of a resulting gear is described by parameters summarized in Table 1. Cutting conditions, listed in Table 2, determine the motion of the workpiece and the hob. Given the spindle speed of a hob, the corresponding spindle speed of the gear is

$$\omega_g = \omega_a / Z_g, \qquad (7)$$

where the number of teeth Z_g of a gear is determined as d/m.

Table 1: Data input of gear geometry into Third Wave AdvantEdge.

Outside diameter (mm)	d_g
Gear height (mm)	W
Module (mm)	m
Pitch diameter (mm)	d

Table 2: Parameters defining hobbing process.

Tool spindle speed (rev/min)	ω_a
Feed per workgear rev (mm/rev)	f_g
Cutting depth (mm)	t
Tilt angle (°)	θ_s
Starting depth (mm)	s

Depending on the starting depth *s*, the cutting positions can be categorized into entry-, full-, and exit-cut. The advanced meshing algorithms in AdvantEdge enable users to start simulations from full-cut positions as shown in Figure 1, which saves a significant amount of computation power.

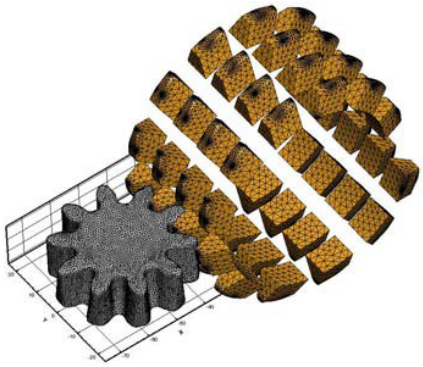

Figure 1: Initial mesh of work gear and hob for the full-cut position.

3. Experimental Setup

To validate the gear cutting predictive model, a series of rack gear milling tests were conducted for Pyrowear X53 steel. The rack gear provides an accurate representation of gear milling performed in industry using solid cutters. Based on the force and chip data collected from the rack gear, the accuracy of the three-dimensional gear cutting predictive model would be understood without over-complication from more complex hobbing paths. All tests were conducted on a Mori Seiki NH3600 horizontal milling machine. Gear steel materials were machined to rectangular test specimens that were then affixed to a Kistler 9255B plate dynamometer as shown in Figure 2.

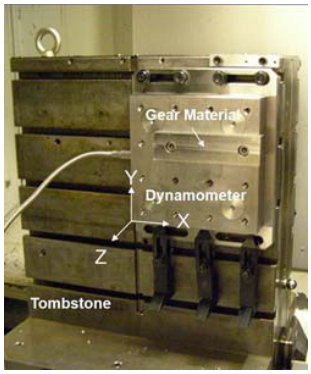

Figure 2: Machine test setup of work gear material machined using a Mori Seiki NH3600.

The cutting tool used in the experiments was a high speed steel gear mill, shown in Figure 3. To prepare the tool for the experiment, the tool was first measured to determine the involute diameter and root diameter of a single tooth. Measurements were completed using an optical microscope and collected from the rake face of the tool. After measurements were collected, the cutter was ground down to only one tooth; this removed run-out inherent in the multiple teeth and improved

dynamometer force output. When fixturing the tool, the involute gear cutter was mounted into the machine spindle on a CAT50 arbor tool holder. The extension of the arbor tool holder allowed the involute cutter to machine the face of the workpiece geometry in the horizontal position. The dynamometer collected force data in the X-, Y-, and Z-axis channels.

Figure 3: Rack gear cutting with a high speed involute cutter ground to a single tooth.

Four sets of cutting conditions were chosen based on industry standards for high speed steel cutting tools in gear steel materials, covering high and low surface speeds and feeds. No coolant was utilized for the experiment. To mitigate the possible influence of wear, cutting tool flank wear was measured between every individual experiment to determine if any of the conditions had damaged the tool or created excessive wear.

4. Model Validation

For the simulations, a single tooth STEP file is imported into the AdvantEdge to form the cutter. The workpiece for simulations starting from the full-cutting position is created though the mesh engine as shown in Figure 4. The initial workpiece mesh consists of 11,712 nodes and 49,412 tetrahedral elements, and the number of elements increases as the cutting progresses due to the adaptive remeshing. The tool spindles about the X axis, and the feed is along the Y direction. Four central processing unit (CPU) cores in the Third Wave high performance computing (HPC) cluster were used for each simulation. The material database implemented in AdvantEdge covers commonly used aerospace and automotive materials.

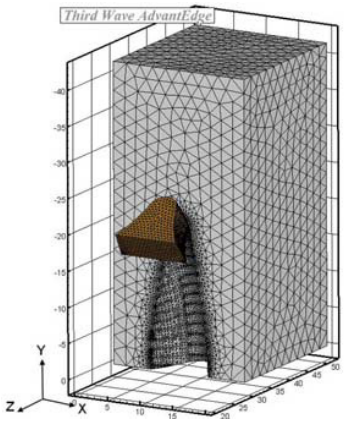

Figure 4: Initial mesh generated by Third Wave AdvantEdge for simulations.

Figure 5 shows the comparison between the predicted and measured forces with Pyrowear X53 at the cutting condition of high surface speed and high feed. A polynomial fit is applied to AdvantEdge predicted forces, resulting in the forces returning to zero at the end of each simulation. It is observed that Y-direction force is higher than the measured force yet close to the upper bound measured in the experiments. The Z-direction force shows close trending between predicted and measured forces. The magnitude of Z-direction force is less than the experimental result before time, around $t = 0.012$ s, and then converges to the measured average force. Figure 6 shows Y- and Z-direction forces for the high speed and low feed cutting condition. Similar observations can be made for the high speed and low feed case.

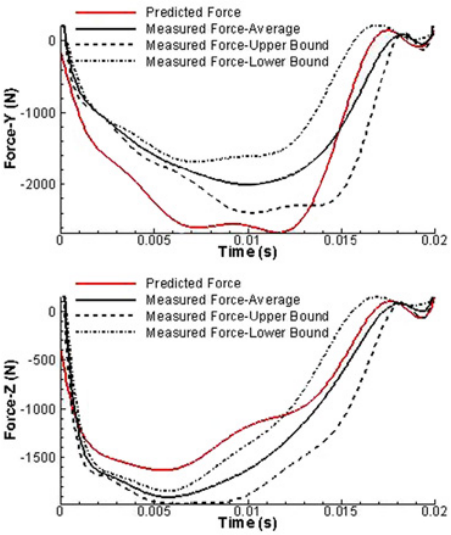

Figure 5: (top) Y-direction and (bottom) Z-direction force comparisons between Third Wave AdvantEdge predictions and experiments for the high surface speed and high feed cutting condition.

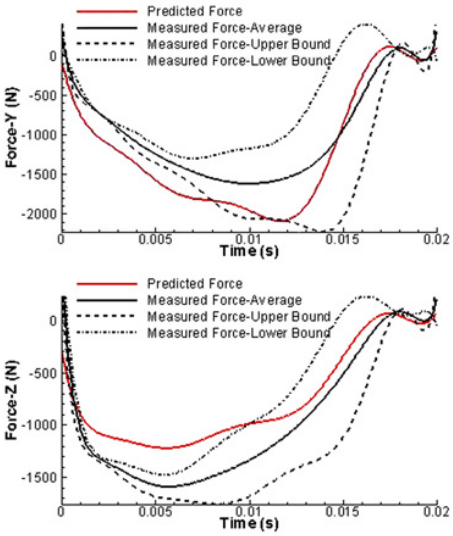

Figure 6: (top) Y-direction and (bottom) Z-direction force comparisons between Third Wave AdvantEdge predictions and experiments for the high surface speed and low feed cutting condition.

The low surface speed cutting is then investigated. The forces are plotted in Figure 7 for the low speed and high feed case. The predicted Y-direction force largely falls between the lower bound and average forces measured in experiments. The Z-direction force in the simulation is lower than the experimental result. Figure 8 shows the force comparison for the low speed and low feed cutting condition. The numerical results show better agreement with the experimental result in the Y direction than in the Z direction. This might be caused by the friction considered in the simulations different from the experimental conditions.

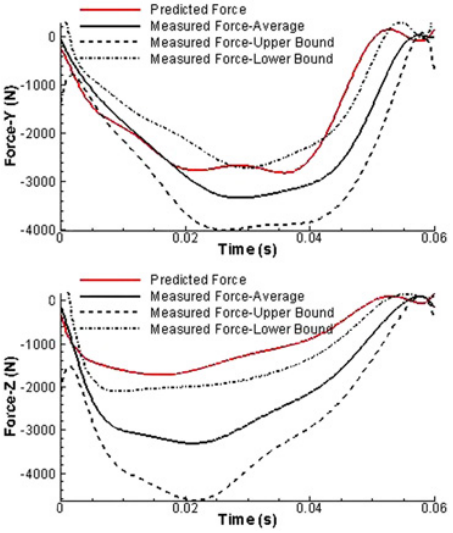

Figure 7: (top) Y-direction and (bottom) Z-direction force comparisons between Third Wave AdvantEdge predictions and experiments for the low surface speed and high feed cutting condition.

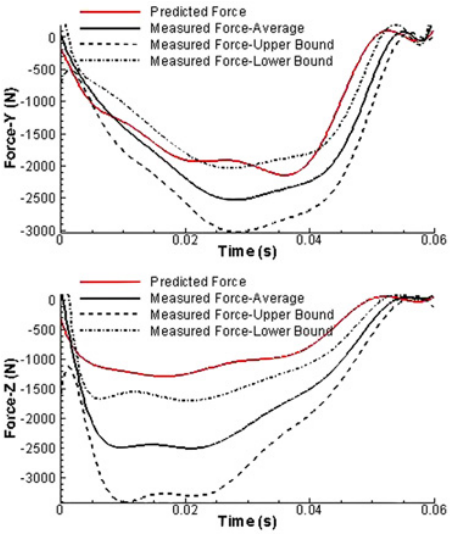

Figure 8: (top) Y-direction and (bottom) Z-direction force comparisons between Third Wave AdvantEdge predictions and experiments for the low surface speed and low feed cutting condition.

Figure 9 shows the simulation of chip formation and temperature distributions on the workpiece and the cutter, which can provide guidance for process improvement and tool optimization. The temperature-time history predicted by AdvantEdge for four sets of cutting conditions is plotted in Figure 10. The peak temperature of high speed cuttings is about 580°C, and 418°C for the low speed cuttings. A comparison of the chip width from AdvantEdge simulation is plotted in Figure 11. Chip width predicted by the simulation is 3.66 mm, which is very close to the experimental value of 3.70 mm.

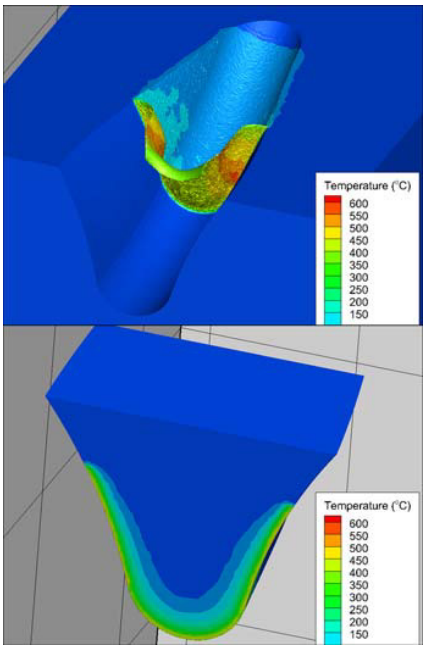

Figure 9: Simulation of chip formation: (top) temperature contour on the chip and workpiece, (bottom) temperature contour on the cutter.

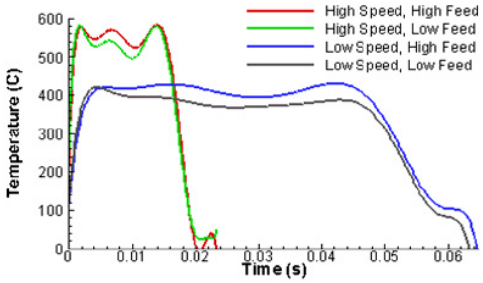

Figure 10: Temperature time history predicted by Third Wave AdvantEdge.

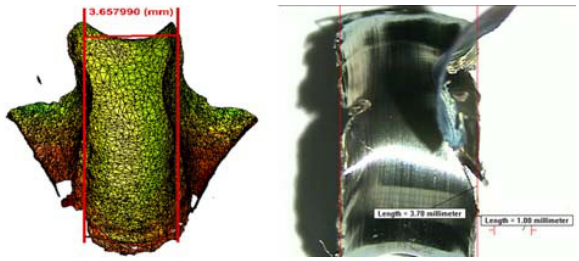

Figure 11: Chip width predicted by Third Wave AdvantEdge compared against chip collected for machining test.

5. Conclusions and Future Work

A finite element-based gear cutting predictive model is presented in this paper. The modeling package is composed of a variety of advanced techniques, including initial meshing that enables simulations to be started from full-cutting positions, three-dimensional kinematics for gear cutting, solution algorithms based on a Lagrangian finite element method, adaptive remeshing techniques, contact algorithms, and nonlinear material models.

To validate the gear cutting predictive model, a series of experiments were conducted for different cutting conditions covering high and low surface speeds and feeds. The simulation results are compared to the experiments. The cutting process is well captured by the predictive model, and good correlations in cutting forces are observed between the predictions and experiments. Due to additional forces observed in the experimental results compared to the numerical simulations in the Z direction, it is expected that further investigation in friction is required. The predicted chip shape is in close agreement with experimental observations. By using the predictive model developed, a better understanding of the gear cutting process can be achieved, and therefore enables process improvement and optimization.

References

[1] Belytschko, T., Liu, W. K., Moran, B., 2001, Nonlinear Finite Elements for Continua and Strutures, Wiley.
[2] Marusich, T. D. and Ortiz, M., 1995, Modelling and Simulation of High-Speed Machining, Int. J. Num. Meth. Eng. 38: 3675-94.
[3] Cuitiño, A. and Ortiz, M., “A Material-Independent Method for Extending Stress Update Algorithms from Small-Strain Plasticity to Finite Plasticity with Multiplicative Kinematics," Engineering Computations, 9 (1992) 437-451.
[4] Man, X., Ren, D., Usui, S., Jonson, C. and Marusich, T.D., 2012, Validation of Finite Element Cutting Force Prediction for End Milling, Procedia CIRP, 1:663-668.
[5] Taylor, L. M. and Flanagan, D. P., “PRONTO 2D: A Two-Dimensional Transient Solid Dynamics Program," Sandia National Laboratories, SAND86-0594, (1987).
[6] Radzevich, S.P., 2010, Gear Cutting Tools: Fundamentals of Design and Computation, CRC Press.
[7] Vasilis, D., Nectarios, V., Aristomenis, A., 2007, Advanced Computer Aided Design Simulation of Gear Hobbing by Means of Three-Dimensional Kinematics Modeling, Journal of Manufacturing Science and Engineering, 129: 911-918.